Research Article | Vol. 26, No. 8 | 16 Apr 2018 | OPTICS EXPRESS 9584
Optics EXPRESS

All-organic switching polarizer based on polymer waveguides and liquid crystals

MANUEL CAÑO-GARCÍA,[1,*] AHMED ELMOGI,[2] MARIE-ALINE MATTELIN,[2] JEROEN MISSINNE,[2] MORTEN A. GEDAY,[1] JOSÉ M. OTÓN,[1] GEERT VAN STEENBERGE,[2] AND XABIER QUINTANA[1]

[1]*CEMDATIC, E.T.S.I Telecomunicación, Universidad Politécnica de Madrid, Av. Complutense 30, 28040 Madrid, Spain*
[2]*Centre for MicroSystems Technology (CMST), imec and Ghent University, Technologiepark 15, B-9052 Ghent, Belgium*
[*]*manuel.c@upm.es*

Abstract: This paper reports on the design, fabrication and characterization of an all-organic photonic integrated circuit working as a switching polarizer for visible light (630nm), combining organic waveguides and liquid crystals that can be electrically driven. The device was made in commercially available epoxy by laser direct writing lithography. A device with a 2dB loss and a 20dB extinction ratio for both polarizations, was simulated; the manufactured devices proved the working principle of the design. The results have led to the design of a switching polarization splitter, in which a careful choice of waveguide material and liquid crystal can lead to devices working on a wide range of wavelengths.

OCIS codes: (130.5460) Polymer waveguides; (130.5440) Polarization-selective devices; (130.4815) Optical switching devices; (130.0250) Optoelectronics.

References and links

1. T. Su, R. P. Scott, C. Ogden, S. T. Thurman, R. L. Kendrick, A. Duncan, R. Yu, and S. Yoo, "Experimental demonstration of interferometric imaging using photonic integrated circuits," Opt. Express **25**, 12653–12665 (2017).
2. S. Feng, C. Qin, K. Shang, S. Pathak, W. Lai, B. Guan, M. Clements, T. Su, G. Liu, H. Lu, R.P. Scott and S.J. Ben Yoo, "Rapidly reconfigurable high-fidelity optical arbitrary waveform generation in heterogeneous photonic integrated circuits," Opt. Express **25**, 8872–8885 (2017).
3. L. Chang, M. H. Pfeiffer, N. Volet, M. Zervas, J. D. Peters, C. L. Manganelli, E. J. Stanton, Y. Li, T. J. Kippenberg, and J. E. Bowers, "Heterogeneous integration of lithium niobate and silicon nitride waveguides for wafer-scale photonic integrated circuits on silicon," Opt. Lett. **42**, 803–806 (2017).
4. D. Liang and J. Bowers, "Photonic integration: Si or InP substrates?" Electron. Lett. **45**, 578–581 (2009).
5. L. A. Coldren, S. C. Nicholes, L. Johansson, S. Ristic, R. S. Guzzon, E. J. Norberg, and U. Krishnamachari, "High performance InP-based photonic ICs - A tutorial," J. Lightwave Technol. **29**, 554–570 (2011).
6. Z. Sheng, D. Dai, and S. He, "Comparative study of losses in ultrasharp silicon-on-insulator nanowire bends," IEEE J. Sel. Top. Quantum Electron. **15**, 1406–1412 (2009).
7. R. Dangel, J. Hofrichter, F. Horst, D. Jubin, A. La Porta, N. Meier, I. M. Soganci, J. Weiss, and B. J. Offrein, "Polymer waveguides for electro-optical integration in data centers and high-performance computers," Opt. Express **23**, 4736–4750 (2015).
8. A. La Porta, R. Dangel, D. Jubin, N. Meier, F. Horst, and B. J. Offrein, "Scalable and broadband silicon photonics chip to fiber optical interface using polymer waveguides," in *Proceedings of the IEEE Optical Interconnects Conference* (IEEE, 2017) pp. 13–14.
9. S. Knauer, M. López-García, and J. G. Rarity, "Structured polymer waveguides on distributed bragg reflector coupling to solid state emitter," J. Opt. **19**, 065203 (2017).
10. S. Chandrasekhar, *Liquid crystals*, 2nd. ed. (Cambridge University Press, 1992).
11. J. Whinnery, C. Hu, and Y. Kwon, "Liquid-crystal waveguides for integrated optics," IEEE J. Quantum Electron. **13**, 262–267 (1977).
12. D. Taillaert, H. Chong, P. I. Borel, L. H. Frandsen, R. M. De La Rue, and R. Baets, "A compact two-dimensional grating coupler used as a polarization splitter," IEEE Photon. Technol. Lett. **15**, 1249–1251 (2003).
13. T. M. Leslie and R. G. Lindquist, "Liquid crystal planar non-blocking nxn cross-connect," (2003). US Patent 6,559,921.

#321324 https://doi.org/10.1364/OE.26.009584
Journal © 2018 Received 1 Feb 2018; revised 8 Mar 2018; accepted 9 Mar 2018; published 3 Apr 2018

Optics EXPRESS

14. J. Leuthold, C. Koos, W. Freude, L. Alloatti, R. Palmer, D. Korn, J. Pfeifle, M. Lauermann, R. Dinu, S. Wehrli, M. Jazbinsek, P. Günter, M. Waldow, T. Wahlbrink, J. Bolten, H. Kurz, M. Fournier, J. M. Fedeli, H. Yu and W. Bogaerts , "Silicon-organic hybrid electro-optical devices," IEEE J. Sel. Top. Quantum Electron. **19**, 114–126 (2013).
15. R. Ding, T. Baehr-Jones, Y. Liu, R. Bojko, J. Witzens, S. Huang, J. Luo, S. Benight, P. Sullivan, J. Fedeli, M. Fournier, L. Dalton, A. Jen, and M. Hochberg, "Demonstration of a low $V_\pi L$ modulator with GHz bandwidth based on electro-optic polymer-clad silicon slot waveguides," Opt. Express **18**, 15618–15623 (2010).
16. C.-T. Wang, Y.-C. Li, J.-H. Yu, C. Y. Wang, C.-W. Tseng, H.-C. Jau, Y.-J. Chen, and T.-H. Lin, "Electrically tunable high Q-factor micro-ring resonator based on blue phase liquid crystal cladding," Opt. Express **22**, 17776–17781 (2014).
17. Y. Xing, T. Ako, J. P. George, D. Korn, H. Yu, P. Verheyen, M. Pantouvaki, G. Lepage, P. Absil, A. Ruocco, C. Koos, J. Leuthold, K. Neyts, J. Beeckman and W. Bogaerts, "Digitally controlled phase shifter using an SOI slot waveguide with liquid crystal infiltration," IEEE Photon. Technol. Lett. **27**, 1269–1272 (2015).
18. A. Elmogi, E. Bosman, J. Missinne, and G. Van Steenberge, "Comparison of epoxy-and siloxane-based single-mode optical waveguides defined by direct-write lithography," Opt. Mater. **52**, 26–31 (2016).
19. E. Hecht, *Optics 2nd edition,* (Addison-Wesley Publishing Company, 1987)
20. P. Cheben, D.X. Xu, S. Janz, and A. Densmore, "Subwavelength waveguide grating for mode conversion and light coupling in integrated optics," Opt. Express **14**, 4695–4702 (2006).
21. K. Kaur, A. Subramanian, P. Cardile, R. Verplancke, J. Van Kerrebrouck, S. Spiga, R. Meyer, J. Bauwelinck, R. Baets, and G. Van Steenberge, "Flip-chip assembly of vcsels to silicon grating couplers via laser fabricated SU8 prisms," Opt. Express **23**, 28264–28270 (2015).
22. D. Cuypers, *Vertically aligned nematic liquid crystal microdisplays for projection applications,* (Ph.D. thesis, Ghent University 2005).
23. E. Otón Martínez, *Adaptive liquid-crystal phase-only passive devices,* (Ph.D. thesis, E.T.S.I. Telecomunicacion (UPM) 2013).

1. Introduction

Photonics integrated circuits (PICs) have many potential applications [1–3] including next generation optical networks. The most employed platforms are silicon on insulator (SOI) and Indium Phosphide (InP) [4]. InP allows for manufacturing of passive and active devices in the same platform technology [5]. On the other hand, the SOI compatibility with CMOS technology leads to excellent processing control, low cost and high volume processing. Furthermore, SOI enables ultra- sharp bends in the optical waveguide, because of their high refractive index contrast [6] allowing for high device density and hence integration level.

Polymer waveguides are in some contexts an attractive alternative platform to SOI and InP due to their intrinsic low propagation losses in the visible and near infrared ranges, their relatively simple manufacturing procedures and their reasonable cost [7]. Nowadays, polymer based PICs are mainly being used as Mode Field Diameter (MFD) adapting interconnections between conventional inorganic densely integrated SOI PICs (small MFD) [8, 9], and telecom fiber (large MFD). Polymer PICs are characterized by a relatively low index contrast, which does not allow realizing sharp bends. However, this reduced contrast also implies larger waveguide dimensions, so that the MFD can be tailored to that of an optical fiber to achieve very low coupling losses. Another possible drawback in some applications may be their limited thermal and environmental stability.

In order to make electronically active organic PICs it is necessary to combine the waveguides with electro-optics materials such as Liquid Crystals (LCs). LCs is a state of matter which is between conventional isotropic liquids and ordered solid crystals [10]. While still being fluid the LCs are optically and dielectrically anisotropic. This means that the spatial orientation of the optical anisotropy (*birefingence*), also known as indicatrix, can be altered with external electromagnetic fields.

In most applications, LC devices are manufactured in such a way that the LC molecules are oriented in a given, *preferred*, direction in the absence of any applied field. By applying an electric field it is possible to switch a LC cell and then let it relax back to a known orientational state, when the electrical field is turned off. Typically the preferred orientation is achieved by

Optics EXPRESS

surface treatment of the inside of the LC cell.

Interestingly, LCs have been used in integrated optics as early as 1977 [11], however low switching speed (ms) has limited the number of LC applications to those where speed was not an issue. Polarization manipulation is an example where speed is not relevant: infact passive devices are often employed [12, 13]. Hybrid devices combining a platform (InP, SOI or polymer) with electro-optic materials can achieve a high efficiencies as shown in various examples using slot waveguides filled with electro-optic materials [14, 15]. LC-based waveguides tuning has likewise been demonstrated [16, 17].

Polarization manipulating devices are not only important for polarization multiplexing and compensation but for polarization-transparent PICs as well [12]. In this work, the design, simulation, manufacturing and characterization of a switching polarizer is presented. The devices is manufactured in a polymer platform employing a cost-efficient laser direct-write lithography (DWL). The active element is created by including a cavity filled with a nematic LC. The cavity is crosses through two parallel waveguides.

This basic design may lead to several devices having different functionalities. As an example, we have also included the design and simulation of a switching polarization beam-splitter.

2. Design and simulation

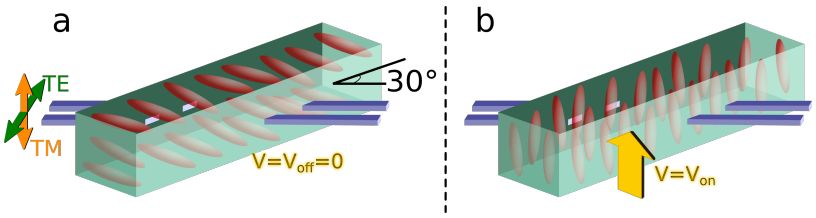

Fig. 1. Sketch of the switching polarizer highlighting the two possible switching states of the LC intersection. The LC-filled trench forms an angle α=30° with the waveguides.

The device consists of two parallel polymeric waveguides made of Epocore (n_{core}=1.590) and Epoclad (n_{clad}=1.578) [18] (Microresist Technology) which are intersected by a trench filled with LC. The trench crosses the WGs at a specific angle to allow polarization dependent switching according to the LC orientation (Fig. 1). Visible light was chosen for the application (630 nm); the device can also be designed for any other wavelength ranges, *e.g.* near infra-red for telecommunications (1300-1600nm). The device splits light into polarizations parallel and perpendicular to the substrate. The chosen LC (MDA-98-1602, Merck KGaA) (n_e=1.78 and n_o=1.52) is a positive LC, *i.e.* the sign of the optical anisotropy, ($n_e - n_o$), and the sign of the dielectric anisotropy ($\varepsilon_e - \varepsilon_o$) are both positive and thus the indicatrix will align parallel to an externally applied electrical field. The trench surfaces are conditioned so that the LC aligns parallel to the substrate plane and perpendicular to the longer trench walls.

Optimal dimensions of the LC intersection were estimated by simulation. As a first approximation, a plane-parallel slab inserted at an angle θ_{wg}, *a slab*, was simulated to calculate the loss caused by the refractive index gap between the polymer waveguides and the LC, and the the beam displacement$d$. The displacement depends on the height (h) of the plane-parallel slab, of the LC refractive index n_{LC} and of the waveguide mode refractive index n_{wg} as shown in Eq. (1) (Fig. 2). The n_{wg} can be calculated using a modesolver. For simplicity, the index here is approximated to $1.58 \approx n_{clad} \approx n_{core}$, as discussed below.

This can be calculated from the waveguide dimensions and n_{core} and n_{clad}.

Optics EXPRESS

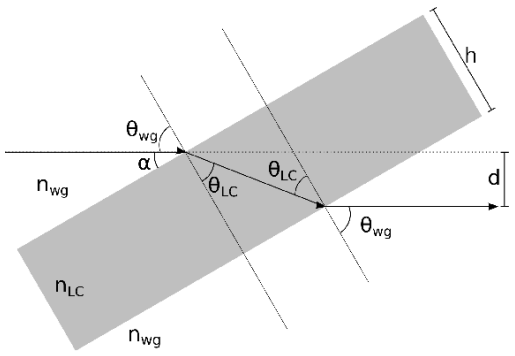

Fig. 2. The displacement of a light beam in a plane-parallel slab.

$$d = h\frac{\sin\left(\theta_{wg} - \theta_{LC}\right)}{\cos\left(\theta_{LC}\right)}; \theta_{LC} = \sin^{-1}\left(\frac{n_{wg}}{n_{LC}}\sin\left(\theta_{wg}\right)\right) \tag{1}$$

Device losses are estimated by computing the reflection intensity at the guide-LC interfaces. At oblique incidence the magnitude of the reflection depends on the polarization of the incident light, *i.e.* whether the light is polarized parallel (P-polarization) or perpendicular (S-polarization) to the plane of incidence, or a linear combination of P and S polarizations. It is important to notice at this point that while in conventional optics P and S nomenclature is used as pseudonyms for TM and TE, the convention when designing pics is that TM describes light with its electric field perpendicular to the substrate, while TE describes light with its electric field parallel to the substrate.

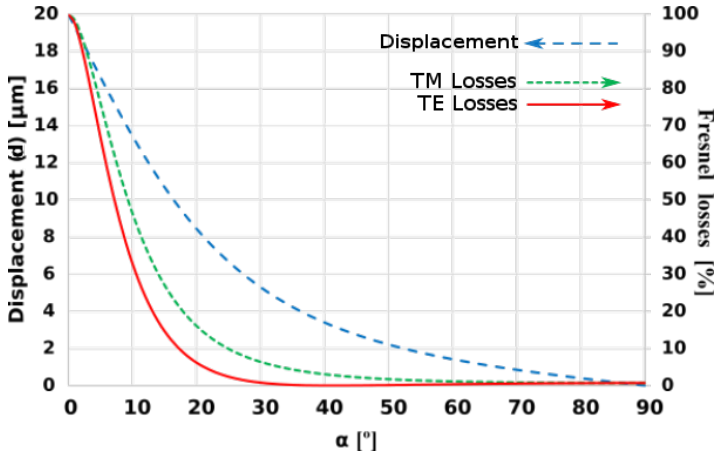

Fig. 3. Simulated displacement and reflection produced by the plane-parallel slab as a function of trench angle α. Blue dashed line: displacement (d). Green dotted line: the TM polarized light losses (Γ_{TM}). Red continuous line: the TE polarized light losses (Γ_{TE}).

The loss Γ caused by the Fresnel reflections at the surfaces for the two polarizations can be cast as Eqs. (2)(3) [19]. The value of the trench width (h) is fixed to 20 μm by fabrication constraints.

Optics EXPRESS

$$R_{TM} = \left| \frac{n_{wg}\cos\left(\theta_{wg}\right) - n_{LC}\cos\left(\theta_{LC}\right)}{n_{wg}\cos\left(\theta_{wg}\right) + n_{LC}\cos\left(\theta_{LC}\right)} \right|^2 ; \; \Gamma_{TM} = 1 - \left(1 - R_{TM}\right)^2 \tag{2}$$

$$R_{TE} = \left| \frac{n_{wg}\cos\left(\theta_{LC}\right) - n_{LC}\cos\left(\theta_{wg}\right)}{n_{wg}\cos\left(\theta_{LC}\right) + n_{LC}\cos\left(\theta_{wg}\right)} \right|^2 ; \; \Gamma_{TE} = 1 - \left(1 - R_{TE}\right)^2 \tag{3}$$

Figure 3 shows the displacement and reflection coefficients for a simulated thickness of 20 μm and refractive indices n_{wg}=1.58 and n_{LC}=1.78, as a function of angle α. A minimum 2.7% reflection is found at 42°, however a trade-off between reflection losses due and the light displacement has been considered, chooseing 30° as the best compromise. At this angle the losses are 5.9% while the displacement is 5.1 μm. Losses increase significantly for angles smaller than 30°.

To complement the above analytical characterization of the initial design, a Lumerical FDTD Solutions finite element simulations were performed, employing the ordinary and extraordinary LC refractive indices n_o=1.52 and n_e=1.78. The simulated thickness of the slab, h, was 20 μm, as above. Being optically anisotropic, both the waveguide design and the LC simulation had to be done for the two perpendicular light polarizations in-plane (TE) and out-of-plane (TM) with the substrate, as well as for the two different switching states of the LC: OFF–aligned in the substrate plane and ON–aligned in the plane perpendicular to the substrate.

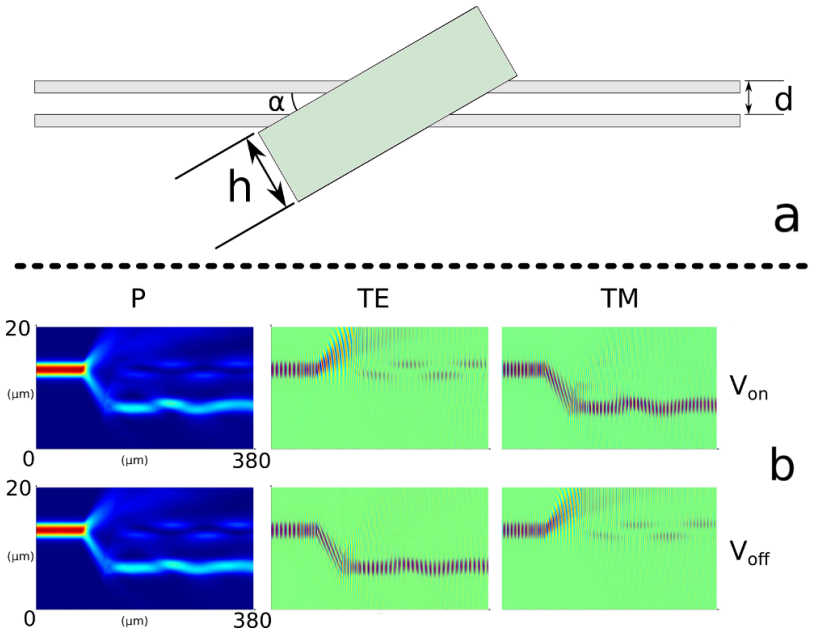

Fig. 4. (a) Scheme of the simulated device with approximate aspect ratio. Various simulations were performed, all with a fixed slab height (h) of 20 μm, trench angle α of 30°, waveguides of 3x3 μm. Separation of the waveguides was varied from 3 to 7 μm; (b) Simulation of the total power and TE, TM field distributions in the central waveguide section for switched and unswitched device with 5 μm waveguide separation. Note that the aspect ratio is not preserved in the simulation images.

Figure 4 shows the simulated light progression for either polarization, in both switching

Optics EXPRESS

states for a waveguide separation of 5 μm. In the switched state, TM polarization propagates with an effective refractive index n_e since the liquid crystal is aligned with the field applied perpendicularly to the substrate plane. The displacement can thus be simulated assuming an exact specific refractive index value *i.e.* n_e=1.78. TE polarization propagates with n_o and since the n_o< n_{wg}, the power in this polarization is refracted away from the output waveguide, upwards in the figure.

In the relaxed state, TM polarization propagates with n_o and is thus refracted away from the output waveguide. TE polarization experiences an effective refractive index n_{eff}, which is between and n_o since light impinges obliquely to the direction of the LC molecules, see Eq. (4). Using our design parameters (90°-θ=α=30° and alignment as in Fig. 1) n_{eff} was calculated to be 1.70. Although this value differs from n_e, the numerical simulation shows that also in this case most of the light is coupled into the output waveguide (see Fig. 4). The same design parameters in the analytical approach lead to significant variation in displacement, *i.e.* 3.8 μm for TE polarization in the OFF state and 5.3 μm for TM polarization in the ON state.

$$n_{eff}^2(\theta) = \frac{n_e^2 n_o^2}{n_o^2 \sin^2\theta + n_e^2 \cos^2\theta} \tag{4}$$

In accordance with this simulation, TM or TE polarization can be transmitted selectively by switching the LC ON and OFF.

It is worth noticing that, only 2 decimals are used in the estimation of both n_{wg}, n_o, n_e and n_{eff}. As seen in the Fig. 5 the displacement (d) of the light beam in the LC, is practically insensitive to any variation in the third decimal of the refractive index. The deviation is below 100 nm per thousands and is easily compensated by a taper structure in the waveguide coupling at the trench [20]. Thus the chromatic dispersion of both the waveguide and the LC will only have marginal relevance for the final device.

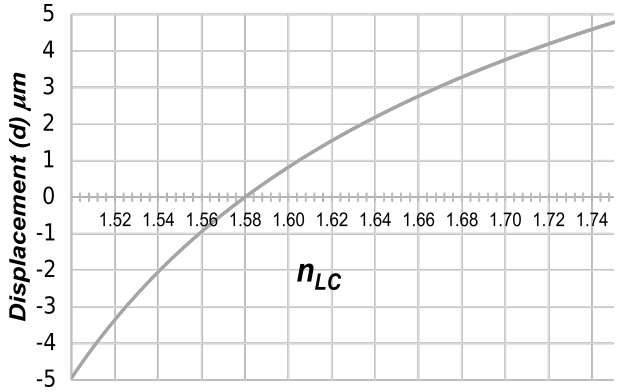

Fig. 5. Analytically calculated displacement and reflection produced by the plane-parallel slab as a function of n_{LC}.

3. Fabrication

LC cells were constructed using a transparent ITO coated glass as top electrode with SiO_2 alignment layer and a metalized silicon wafer as bottom electrode on top of the silicon wafer multiple devices are manufactured in parallel in the polymer layer as seen in Fig. 6. The cross section of each waveguide is 3x3 μm ($n_{TE} \approx n_{TM} \approx 1.585$). Laser ablation is used to carve a 20 μm trench into each device on the wafer as indicated by the two red parallel lines. Prior to assembly, the polymer layer is covered by a SiO_2 alignment layer. When filling the assembled cell, all trenches are filled by the LC.

Optics EXPRESS

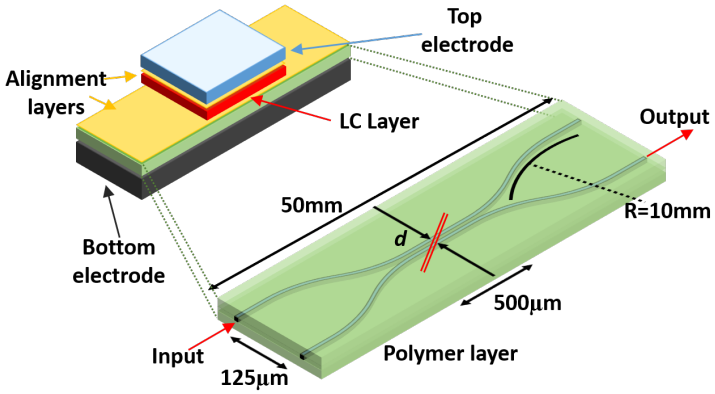

Fig. 6. The basic structure of the developed devices. The input and output ports are indicated.

Organic waveguides were manufactured with DWL. This procedure may lead to significant, systematic, differences between the design and the resulting device. The same issue is relevant to laser ablation used for digging the trench. To account for these, a priori unknown, deviations between design and final device, the same principal device design was repeated on the wafer varying the waveguide separation (d) from 3.5 to 5.5 μm. 20 different devices were designed and manufactured.

Table 1. **Optimized process parameters for the waveguides fabrication.**

Process Step	Epoclad 50	Epocore 2
Spin coating	5000 rpm 1'	1900 rpm 30"
Soft bake	5'@50°, 5'@90°, 10'@120°	5'@50°, 5'@90°, 10'@120°
UV exposure	1'@10mW/cm^2	DWL @ 334mJ/cm^2
Post exposure bake	15'@90°	2'@50°,4'@90°
Wet development	-	45" in mr-Dev600, 1' rinse IPA
Hard bake	90'@120° in oven	90'@120° in oven

Each device consists of a pair of parallel Epocore/Epoclad (Microresist Technology) [18] polymeric waveguides (n_{core}=1.590, n_{clad}=1.578). An excimer laser (KrF, working at 248 nm,

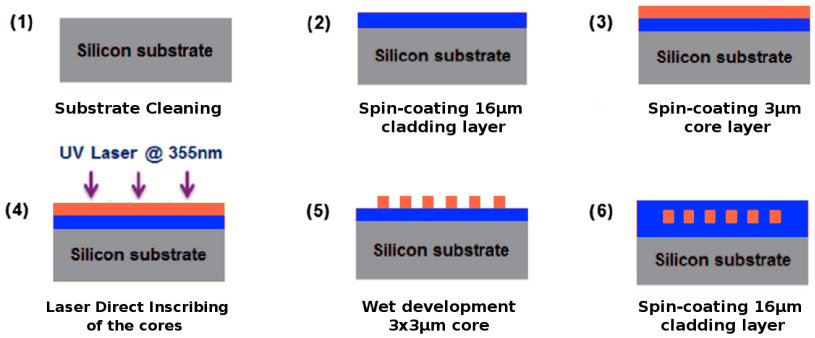

Fig. 7. Steps to fabricate the waveguides.

Optics EXPRESS

pulse duration 5-8 ns, pulse energy 570 μJ)) was used to carve the trench. The trench was filled with MDA-98-1602 (n_e=1.78 and n_o=1.52).

The waveguide manufacturing is illustrated in Fig. 7 and described in [18]. Table 1 summarizes the optimized process fabricationn parameters. Once the waveguides are manufactured, the trench is made directly in the polymer sandwich by ablation. An excimer laser was to ablate the complete clad-core-clad stack. The excimer laser beam passed a rectangular mask (2000 μm x 200 μm) and the de-magnified image (factor of 10) of the mask was projected onto the polymer coated sample. This technique has been optimized in the past to make angular cuts [21]. 70 pulses with a ablation rate of 0.45 μm/pulse were applied to carve the desired trench in waveguide core.

The last step is making the LC cell. LC alignment in absence of any external field was conditioned by an SiO_2 layer deposited by oblique thermal evaporation (50 nm with an angle of 45°) onto the polymer layer and trenches and onto the top electrode [22]. 5 μm spacers were deposited onto the SiO_2 alignment layer on the top surface, so that the LC could flow freely and fill all the trenches on the chip. A gasket seal was applied leaving a mouth open for vacuum filling as described in [23], A sketch of the final macroscopic structure is shown in (Fig. 6).

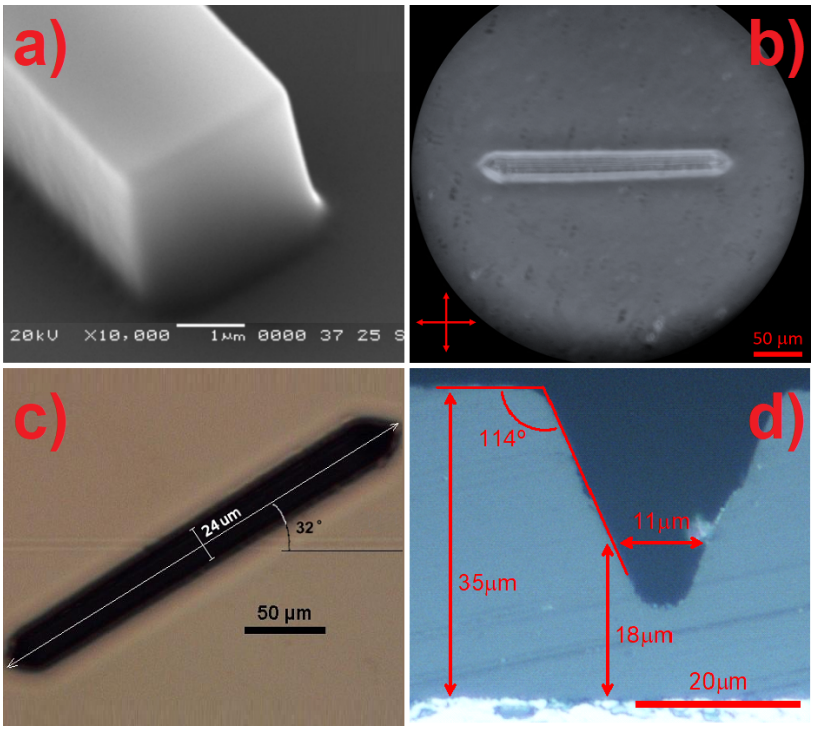

Fig. 8. a) SEM image of the a waveguide without cladding; b) optical microscope image of a trench with LC between crossed polarizers. c) optical microscope image of the empty trench. d) optical microscope image of the cross section of a trench.

SEM was employed to assess the quality of the waveguides, see Fig. 8(a). These are well defined rectangular shapes. The roughness of the bottom and the top cladding has been previously measured to be 2.2 nm [18].

As a result of unexpected high losses, the LC alignment and the quality of the trench cut was assessed. The device was observed between crossed polarizers with the predetermined orientation aligned with one of the polarizers, (Fig. 8(b)). Light transmission inside the trench is as low as the transmission outside the trench, indicating a good LC alignment. The trench walls themselves cause some light scattering. A trench angle with respect to the waveguide of

Optics EXPRESS

32° was measured(Fig. 8(c)), which was 2° rotation with respect to the design. Furthermore, the cross-section of the trench (Fig. 8(d)) revealed that the cut was not a rectangular section perpendicular to the substrate surface, but rather a V-shaped cut. For wider laser-ablated trenches, typically only 5-10° deviation from 90° cuts are expected [21], but in our case the trenches came out with almost 25° deviation (114° instead of 90°) due to the desired high aspect ratio and thin trenches. The resulting trench is thus thinner as is the effective LC slab. At the height of the waveguide the LC slab is only 11.3 μm, 8.7 μm less than the desired value. As a result a smaller displacement is expected and thus the devices with smaller waveguide separations are expected to give the best results. Additional losses were added by the not normal ablation (~3 dB for the TM and ~1 dB for the TE).

4. Optical characterization, results and discussions

As mentioned before, several devices were made on the same chip to account for manufacturing tolerances. The devices differ in the distance between the waveguides at the position of the LC slab. Devices with separations ranging from 0.9μm to 2.5μm *i.e.* ([3.9-5.5]μm between center of the waveguides) in steps of 0.1μm were successfully manufactured.

Two chips with duplicated design were characterized. No noteworthy difference between the four repetitions was found.

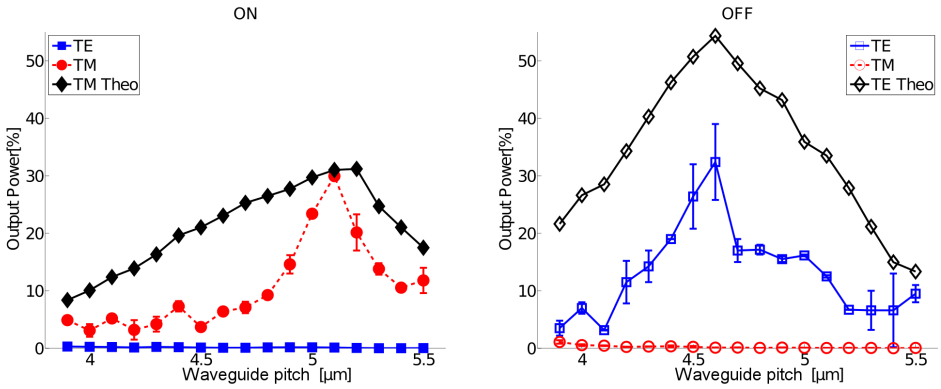

Fig. 9. TM/TE intensities at the output port for the two different LC switching states. The measured values allowed for an estimation of the effective refractive indices, $n_{eff_{TM}}$ and $n_{eff_{TE}}$, for the on and the off switching states. These derived values were used in in the calculation of the simulated transmission curves. The measured intensities are relative to the power transmitted in a straight waveguide.

A polarized laser diode emitting at 630 nm coupled to a single-mode fiber reel was used in the characterization of the device. The light was coupled into the waveguide using a nano-positioner (*Thorlabs NanoMax XYZ*). A fiber rotator was used to manipulate the polarization at the input of the device. The light at the device output is captured using a multi-mode fiber and a photo-detector.

Figure 9 shows the relative power transmission versus waveguides separation for the two input polarizations (TM, TE) with LC switched (V_{on}) and unswitched (V_{off}). The device works as a switching polarizer. When the applied voltage is off the TE polarization is guided to the output port. When the applied voltage is on the TM mode is guided to the output port. Each of the polarizations has an optimal waveguide separation for maximum transmission to the output port. This is due to the fact that the effective refractive index of the LC for TE is smaller that for TM ($n_{eff,TE} < n_{eff,TM} \approx n_e$). The unswitched LC alignment is not perpendicular to the TE mode propagation (see Fig. 1), but the switched LC alignment is almost perpendicular to the TM mode propagation. The slight deviation (less than 3°) is caused by the non-vertical trench sides.

Optics EXPRESS

Waveguide separation of 4.9 μm provides a measured power transmission of more than 15% for both polarizations when they are guided to the output port depending on the switching state of the LC. Simulations of the structure taking the trench imperfections into account were performed and the effective refractive indices for $TM_{V_{on}}$ and $TE_{V_{off}}$ were refined so that the simulated maximum transmission waveguide separation corresponded to the measured maximum transmission waveguide separation in the output: $n_{eff}\left(TM_{V_{on}}\right) = 1.72$ and $n_{eff}\left(TE_{V_{off}}\right) = 1.69$. In the case of $TM_{V_{off}}$ and $TE_{V_{on}}$, a refractive index n_o has been employed. A reasonable fit between the simulated and the measured values was obtained (Fig. 9).

With a perfectly rectangular trench the simulated loss was around 2 dB. The actual loss is ≈8 dB, this higher loss is attributed to the reflections in non-perpendicular surfaces and mode expansion in the trench . This could be reduced making a perpendicular cut and including a taper in the *coupling-in-section* of the trench zone [20].

5. Proposed advanced devices

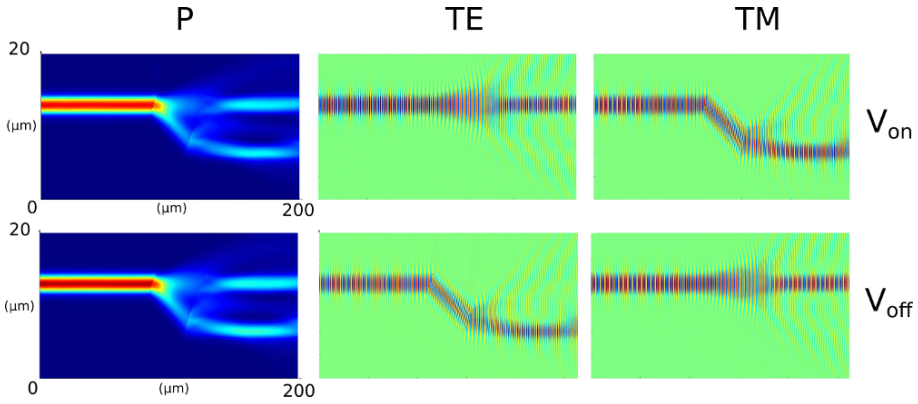

Fig. 10. Simulation of the designed wide wavelength switchable optical polarization splitter. The total power and TE, TM field distributions in the central waveguide section for switched and unswitched device with 6 μm waveguide seperation. The trench size was 20 μm and the LC refractive indeces varies between n_o=1.58 and n_e=1.78.

Based on the above device a switching polarization beam splitter can be proposed.

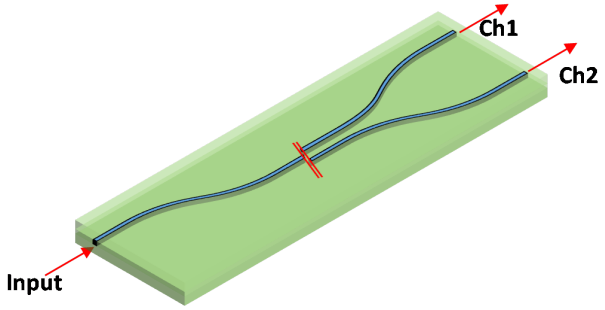

Fig. 11. The fundamental design of a switching polarization splitter using the MDA-98-1602. In this case neither of the two output ports can be aligned with the input port since $n_o < n_{wg}$.

Choosing an LC with an ordinary refractive index n_o=n_{wg}=1.58 the same geometry will lead to a switching polarization beam splitter where the waveguide separations and slab height depend

Optics EXPRESS

on n_e. Fig. 10 shows a simulation of the power distribution of the two polarizations for the two switching states in a device identical to the one above but with different parameters: n_e=1.78, n_o=1.58, $\alpha = 30^\circ$ and h=20 μm. The working principle is the same as above, but in this case the both polarizations are guided for both switching states.

Alternatively, a switching polarization splitter may be manufactured using discontinuous waveguides (Fig. 11) while maintaining the LC and LC alignment as in the original design. In this case the trench positioning becomes critical since it has to be situated right at the discontinuity of the waveguides. The simulation of this device would be similar to the simulations shown in in Fig. 4(b), but with an upper waveguide located at the position whereto the TE(V_{ON}) and TM(V_{OFF}) modes are being refracted.

6. Conclusion

A liquid crystal slab inserted in a tilted trench in the light path of two waveguides has been shown. This simple device has demonstrated several functionalities depending on the tilt angle, the refractive indices of the waveguides, the liquid crystal and the relative position of the output and input waveguides. Some examples are polarizer, optical switch and polarization splitter switch.

These functionalities have been confirmed by simulations with Lumerical FDTD. Quite moderate losses (2 dB) are predicted, making the device potentially useful for practical applications.

Actual devices based on organic waveguides have been demonstrated in the visible region. Extension to NIR wavelengths is straightforward, since no restrictions in the spectral range –other than waveguide limits– are expected. NIR range is better attainable with inorganic waveguides; the system is fully compatible with these waveguides.

The integration level of photonic integrated circuits (PICs) is far from that of electronic integrated circuits. Devices like the ones presented result in tuneable structures that may significantly increase the PIC functionality without adding much complexity, and thus contributing to the development of more integrated/sophisticated circuits.

Funding

Spanish Ministerio de Economía y Competitividad (RETOS TEC2013-47342-C2-1-R, RETOS TEC2016-77242-C3-2-R, BES-2014-070964, EEBB-I-17-12110); Comunidad de Madrid and the European Structural Funds (S2013/MIT-2790 SINFOTON-CM).

Acknowledgments

Authors are grateful for financial support. Manuel Caño-García is specially grateful for the help provided by the CMST support team.